

# Regolith Particle Erosion of Material in Aerospace Environments

Emma Bradford  
Mars 2020 Materials Engineering, Test &  
Evaluation  
Jet Propulsion Laboratory, California  
Institute of Technology  
Pasadena, CA, USA  
Emma.M.Bradford@jpl.nasa.gov

Jason Rabinovitch  
Entry, Descent & Landing and Formulation  
Jet Propulsion Laboratory, California  
Institute of Technology  
Pasadena, CA, USA  
Jason.Rabinovitch@jpl.nasa.gov

Mohamed Abid  
Mars 2020 Deputy Chief Mechanical  
Engineer  
Jet Propulsion Laboratory, California  
Institute of Technology  
Pasadena, CA, USA  
Mohamed.M.Abid@jpl.nasa.gov

**Abstract**— This paper studies the effect of exposing thermal control S13GP:6N/LO-I white paint, Kapton flex cable, fiber optic cable, HEPA filter, and M55J graphite composite to high-velocity regolith environment that spacecraft landing on Mars are commonly exposed to. Due to the similarity between the Mars 2020 Rover design and Mars Science Laboratory design, it is expected that the Mars 2020 rover will be exposed to a similar high-speed regolith environment that the Mars Science Laboratory was exposed to. This environment is replicated to test the survivability of susceptible materials. The testing is performed at the University of Dayton Research Institute in Dayton, Ohio. The experiments expose different materials to basaltic-like particles ranging in size from approximately 40  $\mu\text{m}$  to 2 cm, at velocities ranging from 19 m/s to 250 m/s, with varied particle fluxes (measured in  $\text{mg}/\text{cm}^2$ ). Depending on the size of the particle used, the particles can either embed in or erode the material. Post-test analysis shows that all materials tested will survive the expected environment observed during the Mars 2020 landing event. Some materials are tested to failure in order to better characterize material response. Materials that fail in some test scenarios include the paint, fiber optic cable, and the graphite composite. After being exposed to regolith, the  $a/\epsilon$  ratio of the paint increased by  $\sim 37\%$  due to particles embedding in the paint. Darkening of the paint can negatively affect thermal control of the rover. With high particle mass fluxes, the paint eventually degraded enough to expose the aluminum substrate. When impacted by a 1.5 cm particle traveling at 20 m/s, the fiber optic cable did not sever, but the impact did cause the cable to deform enough to crack the glass, which resulted in a significant increase in attenuation, rendering the cable unable to transmit data. The graphite composite also failed when exposed to high particle fluxes. All of the observed failures occurred for test cases above the expected landing environment with significant margin. Tests performed beyond the requirements help characterize how well these materials will survive in even more extreme environments for future missions.

**Keywords**—Mars, erosion, thermal control paint, fiber optic cable, composite, flex cable, HEPA, M2020, and MSL

## I. INTRODUCTION

During the landing phase for the Mars Science Laboratory (MSL) and Mars 2020 (M2020), the Mars Landing

Engines (MLEs) produce high velocity gas plumes that will interact with the Martian surface. The velocity and density of the gas in the MLE plumes is high enough so that significant entrainment of surface regolith into the flow will occur [1]. A complex flow field develops due to plume/plume and plume/surface interactions (Fig. 1) [2]. The entrained particles may impact the rover and have the potential to cause damage to exposed surfaces and hardware [3]. Images taken immediately after MSL landed show particles ranging in size from approximately 0.3 – 2 cm deposited on the top deck of the rover, and it is presumed that these particles were deposited on the rover during the landing event [4]. Furthermore, the wind sensor in the Rover Environmental Monitoring Station (REMS) instrument failed after MSL landed, and it is hypothesized (though not confirmed) that the MSL dust environment during landing damaged this instrument.

The M2020 rover is a heritage design based on MSL. While many aspects of the MSL and M2020 spacecraft designs are similar, the M2020 spacecraft accommodates an updated instrument suite, which has caused the two designs to diverge in some places. However, the MSL and M2020 Entry, Descent, and Landing (EDL) sequences and architecture are very similar (Fig. 2), which means that the M2020 rover will also be subject to a dust environment during landing that has the potential to cause damage to exposed systems [5]. Both the MSL and M2020 missions paint the majority of the exposed rover surfaces white for passive thermal control. MSL used Aptek 2711, a white inorganic paint for this purpose, while M2020 will use a different paint. In 2008, the MSL team tested representative Aptek 2711 paint coupons in a simulated dust particle environment [1]. Both the durability of the paint and the change in optical properties of the paint was measured after the coupons were exposed to a known mass flux of particles. For M2020, a silicone based S13GP:6N/LO-I (S13) paint from Alion Science is used, due to unavailability of the Aptek paint previously used on MSL. While these are both white paints, the Aptek 2711 and S13 paints have different physical properties: Aptek 2711 is prone to chipping, while S13 is soft and prone to peeling and particle embedment (Table I). S13, when exposed to a high-speed particle environment is predicted to behave

NASA funded the research for this paper.

© 2018 California Institute of Technology. Government sponsorship acknowledged  
XXX-X-XXXX-XXXX-X/XX/XXX.00 ©2019 IEEE

very different from Aptek 2711 based on its chemical composition. Aptek 2711 is prone to losing material slowly as observed during the MSL test campaign [3]. In order to demonstrate S13's erosion resistance, additional erosion tests are required for M2020. The M2020 testing is expanded in order to include additional sensitive hardware exposed on the rover (flex cable, fiber optic cable, M55J composite, and HEPA filter) that could potentially be damaged by particle strikes during the landing event.

TABLE I. POTENTIAL FAILURE MODES OF PAINT

Potential Failure Modes	Aptek 2711 (MSL)	S13 (M2020)
Peeling	Low	High
Sticking/Embedding	Low	High
Pitting	High	Medium
Cracking	High	Low
Chipping	High	Low

## II. BACKGROUND

The determination of the test parameters used in this study is out of scope for this work. However, the M2020 mission has requirements declaring the necessity to survive regolith impacts, and verification of these requirements must be performed by either analysis or test. The particle velocities and mass flux values that make up these requirements are based on a worst-case analysis using models derived by Hutton and Roberts that were originally used to predict plume/surface interactions on the Moon for the Apollo missions [5-8], and extended to MSL/M2020 conditions.

While Computational Fluid Dynamics (CFD) simulations have been performed in the past in order to predict the MLE plume diameter to make sure that the hot plumes do not damage the rover, state-of-the-art computations are currently unable to resolve and predict the complicated fluid/particle interactions that are present during a real rover landing on Mars (Fig. 3). Some qualitative observations can be made from previous CFD simulations (with no particles) which can help inform the test plan. As expected, CFD simulations show that the bottom and sides of the rover have the most exposure to the MLE plumes. However, based on MSL data it is believed that particles impact the top deck as well. This was seen in some of the first images MSL took after landing on Mars on Sol 2 of its mission (Fig. 4). Both sand and rocks are seen scattered on the top deck of the rover. The largest particle observed on the top deck was ~2 cm in diameter. The M2020 test conditions (primarily particle size range) are informed by the particles observed on the MSL rover post-landing. Unfortunately, MSL rover images give no quantitative information on the flux of particles that contacted the rover during landing. Due to several unknown variables assumed for these analyses, the test conditions are picked based on conservative estimates of what the particle environment will be.



Fig. 1. MSL EDL Instrument (MEDLI) suite camera images showing the MLE plumes starting to erode Martian regolith at approximately 63 meters above the surface (blue square) [1].

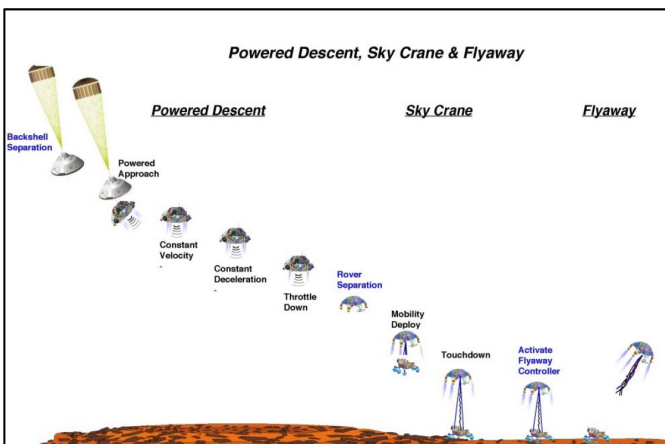


Fig. 2. The MSL Entry, Descent, and Landing (EDL) sequence [3].

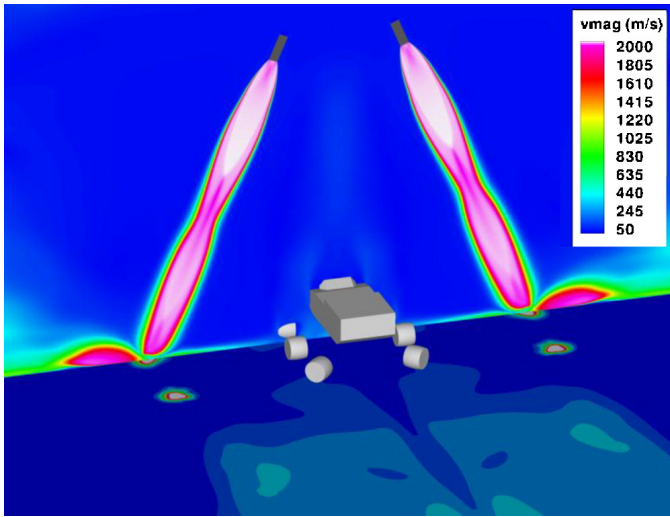


Fig. 3. CFD simulations demonstrating plume-plume interactions and plume-rover interaction [2]. The color scale represents gas velocity.



Fig. 4. Images taken by MSL on Sol 2 show the top deck scattered with particle debris after landing, some almost 2 cm in diameter [4].

### III. TEST EQUIPMENT

Both the MSL and M2020 test campaigns took place at the University of Dayton Research Institute (UDRI). UDRI uses three different types of equipment in order to test over a range of particle sizes, velocities, and mass fluxes: 1) a Particle Erosion Rig, 2) a Gravelometer, and 3) a Gas Gun. A comparison of all equipment can be found in Table II along with media variations. The media used in this test campaign is chosen to be as similar as possible to regolith on Mars, though equipment and facility considerations are taken into account as well.

The Particle Erosion Rig is used for testing helicopter rotor blades per MIL-STD-3033 [9], and the set up is modified for the M2020 test. The Particle Erosion Rig uses pressurized gas to accelerate a constant stream of particles through a nozzle towards a test sample (Fig. 5). A Laser Doppler Anemometer (LDA) setup is used to measure particle velocity. This test apparatus allows the particle velocity, particle size, impact angle, and mass loading to be varied as desired. Mass loading is defined to be the total mass of particles that impact a test article per unit area (which is a function of particle mass loading, velocity, and time), and has units of mass per unit area. In this work  $\text{mg}/\text{cm}^2$  are used for convenience [10]. The gravelometer is generally used for testing motor vehicle coatings per ASTM D1370 [11], and uses pressurized gas to accelerate a steady stream of particles up to speed before they impact samples (Fig. 6). However, for the M2020 test, the gravelometer equipment was altered from the ASTM standard and the LDA was used to measure the velocity of the particles. The Gas Gun uses pressurized air to launch one particle at a time at the sample, using a large barrel in order to launch larger particles (Fig. 7). The particles used in the Gas Gun are shown in Fig. 8. Velocity of the particles from the Gas Gun is measured with LDA as well. Table II compares the media type used for each test.

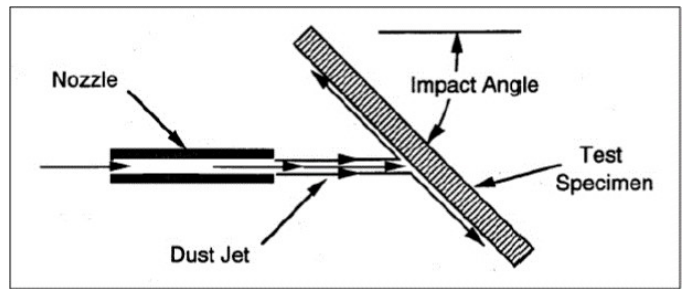


Fig. 5. Schematic for the Particle Erosion Rig [10].

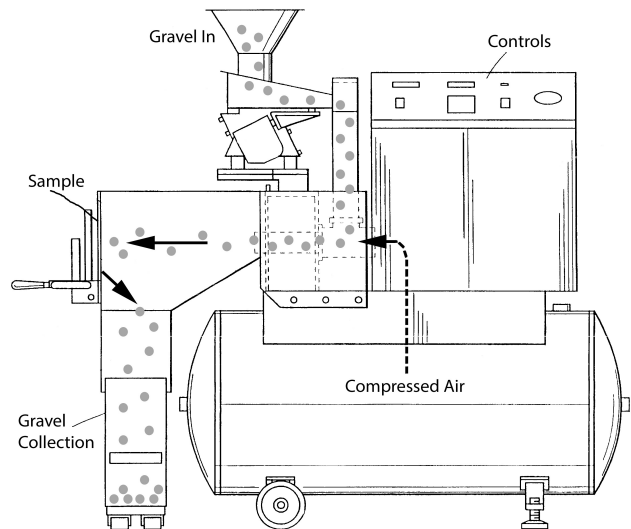


Fig. 6. Schematic for Gravelometer [12].

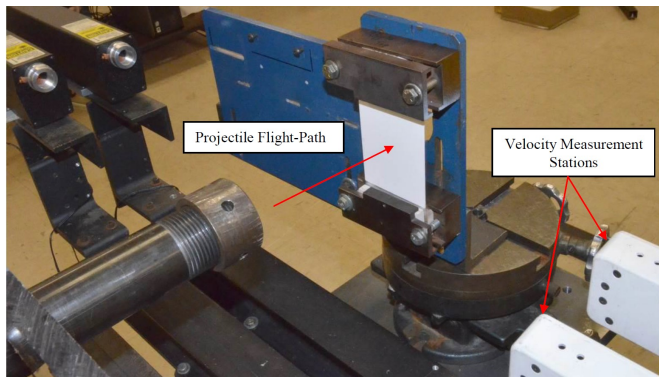


Fig. 7. Test configuration for the Gas Gun with 76.2 mm x 127mm samples.



Fig. 8. An image of the various size Tonalite rocks used in the Gas Gun, both ends of the rock are formed to a 118° angle.

TABLE II. TEST APPARATUS AND MEDIA USED

Test Apparatus	Erosion Rig		Gravelometer	Gas Gun
Nomenclature	SAND		GRAVEL	ROCK
Material	Quartz		Basalt	Tonalite
Test Media	Foundry Sand	Golf Sand	Mojave Mars Simulant (MMS) [13]	Cedar City Tonalite
Particle Size	38-44 $\mu\text{m}$	170-550 $\mu\text{m}$	1-10 mm	6.4-15.8 mm
Density	2.5 g/cm <sup>3</sup>	2.5 g/cm <sup>3</sup>	2.5 g/cm <sup>3</sup>	2.5 g/cm <sup>3</sup>
Color	brown	brown	red/dark gray	brown
Shape	round	sharp and angular	Irregular	machined to a 118° point

#### IV. MATERIALS

The materials are selected based on risk analysis performed by each of the M2020 rover subsystems engineers and reviewed by a material engineer. Materials with a single point of failure and high likelihood of particle impact are selected for testing. Six materials meet this criteria along with the S13 painted on 7075 Aluminum: Kapton flex print, jacketed Fiber Optic Cable (FOC), M55J graphite fiber composite, and HEPA (High-Efficiency Particulate Air) filter. The Kapton flex print is flat electrical cabling used on the rover and is exposed to the particle-entrained environment in multiple locations,

such as the Remote Sensing Mast (RSM) (Fig. 9), and the robotic arm. Damage to the trace, through either a short circuit or an open circuit, of the flex cable from particle impacts could cause electrical problems for the specific instrument of interest.

The SuperCam instrument, located on the RSM uses the FOC and a laser system to provide chemical composition analysis of geological samples. During landing, the rover mast is stowed to protect the camera, but the FOC is exposed in several locations (Fig. 9). Damage to the FOC would result in complete loss of remote chemical analysis capability, remote Raman mineralogical capability, and remote visible reflectance spectroscopy. Without the FOC, SuperCam would only have the ability to image and measure IR spectroscopy. In flight, the FOC is mounted in different configurations, including in some locations, loosely and with no cover. This configuration was replicated for the testing, in order to allow the FOC to move freely, meaning the main failure mode for the FOC would be a rock hitting the cable and causing it to bend more than the manufacture recommended maximum 2-inch bend radius. Bending to this extent would cause the glass to crack, rendering the cable inoperable.

M55J is a graphite fiber composite with BTCy-1 resin, 4 plies thick, and is fabricated at Lockheed Martin. The primary use of this material is to cover the Mars Helicopter (a technology demonstration), which is stored beneath the rover during landing. This cover will act as a debris shield for the helicopter during landing. The minimum clearance between the shield and the helicopter is 6.35 mm (0.25 inch). If the composite were to have a deformation exceeding the clearance value, or experienced structural failure, the performance of the helicopter could be affected in a negative manner.

The rover uses HEPA filters to allow the internal rover structure to equalize pressure with the Martian atmosphere quickly, while preventing contamination, either through Earth-based microbe egress or through Martian dust ingress. This poses a planetary protection risk, rather than a functional risk because filter failure can result in microbial contamination of Mars. Extreme caution is taken during fabrication to ensure cleanliness, and the HEPA filters are used as an additional precaution. There are no operational concerns with filter clogging; material damage is the sole risk. The flight assembly consists of the HEPA material inside of an aluminum housing, with the HEPA filter is covered with a wire mesh containing 2mm holes, whose purpose is to provide some protection from the larger particles; however, it will still allow the smaller particles pass through.

S13 paint covers almost all exposed rover surfaces and thus has a high likelihood of particle impact. The white paint facilitates passive thermal control through radiation, with the top deck of the rover acting as the primary heat rejection surface. There are a few locations on MSL where paint chipping has been observed (Fig. 10), but the major concern is the accumulation of dust on the top deck. Images of the top deck taken over MSL's mission life show sand migration (e.g. accumulation and subsequent dissipation) (Fig. 11); both erosion and dust coverage will affect the optical properties of the white paint. As the  $\alpha/\epsilon$  ratio increases due to either paint

removal or dust coverage, the temperature of the rover will increase. While there is the possibility that a Martian wind will blow off the dust, or that vibrations from driving will knock particles loose from the top deck, for particles embedded in the paint, the likelihood of particle migration from these sources is minimal.

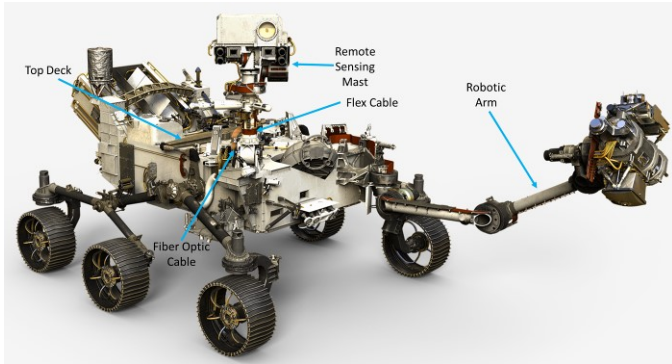


Fig. 9. Overall of the M2020 rover [14].

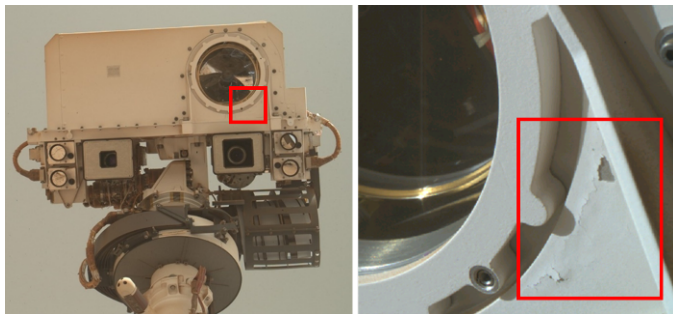


Fig. 10. Images taken MSL showing evidence of the ApteK 2711 chipping [4].



Fig. 11. This series of images taken by MSL of the sundial throughout the mission show particle migration, dust accumulates and then the wind causes the dust to dissipate and this cycle is repeated [4].

Seventy-Five 25.4 mm x 25.4 mm<sup>5</sup> paint coupons of 7075 Al were prepared with SS-4044 primer and X-99 thinner. Once the paint is fully cured, the coupons undergo a vacuum bakeout at 110°C for 72 hours at less than 6x10<sup>-3</sup> Pa. The painting process and bake out for the coupons is identical to the process that the M2020 flight parts will undergo. ApteK Laboratories Inc. provided several paint samples of 2711, in order to have samples to compare with the previously performed MSL testing [3]. Paint coupons with xylene are also prepared to investigate qualifying new primers and xylene thinner combinations (4044-xylene and 4155-xylene), with the properties listed in Table III. The xylene thinners will not be used on M2020 due to qualification concerns, but is possible that xylene thinners will be considered for future missions. For

this test campaign, a paint thickness of 0.10-0.15 mm is used for all paint coupons. Optical measurements are taken with a calibrated TESA 2000, AZ Technology Portable Emisometer/Reflectometer and Solar Reflectometer, which measures total hemispheric reflection. This instrument has a measurement error of 3%. Thickness measurements are made with a calibrated Elcometer 311 Coating Thickness Gauge.

TABLE III. PRE-MEASUREMENTS OF THE PAINTS

	Average Absorptivity	Average Emissivity	$\alpha/\epsilon$	Average Thickness (mm)
X-99 S13 Paint	0.17	0.87	0.20	0.13
ApteK 2711 painted in 2017	0.16	0.83	0.19	0.13
ApteK 2711 painted in 2008 [3]	0.16	0.83	0.19	0.05
4044 Xylene S13 Paint	0.21	0.9	0.23	0.10
4155 Xylene S13 Paint	0.2	0.91	0.22	0.13

## V. TEST PROCEDURE

The test parameters (Table IV) were selected to represent as best as possible the predicted landing environment with margin, while staying consistent with facility capabilities. All of the test are preformed in ambient Earth temperature and pressure. Some samples are tested to failure (beyond the original requirements) to fully characterize the material and to determine failure mechanisms where possible. The 25.4 mm x 25.4 mm coupons are placed in a recessed box, with a <25.4 mm diameter hole on the bottom side, which protects the edges of the coupons. Sixteen 25.4 mm x 25.4 mm samples are tested per run on the Particle Erosion Rig (Fig. 12). Pre-Post functional tests are preformed on all materials (Table V). This table displays the different parameters each material was tested to. Tables IV and VI summarize all of the tests performed in this campaign.



Fig. 12. Test configuration for the 1"x1" samples, front and back. The 1"x1" coupons were placed in a recessed box, with a <1" diameter hole on the bottom

side, which protected the edges of the coupons. Sixteen 1"x1" samples could be tested per run on the Particle Erosion Rig.

TABLE IV. TEST MATRIX

Test Apparatus:	Erosion Rig								Gravelometer	Gas Gun					
Particle Size:	38-44 μm			177-250 μm			240-550 μm		1-10 mm	9.5 mm	12.7 mm	15.8 mm			
Velocity:	250 m/s			160 m/s	80 m/s			85 m/s		25 m/s	20 m/s	22 m/s	22 m/s	25 m/s	
Impact Angle:	30°	60°	90°	30°	30°	90°	30°	90°	90°	90°	90°	90°	30°	90°	
MATERIALS	S13 Paint	X	X	X	X	X	X	X	X				X	X	
	Aptek 2711 Paint				X										
	Xylene Paint				X				X						
	Flex Cable						X	X	X	X				X	
	M55J Composite						X	X	X	X				X	
	HEPA Filter						X	X	X	X					
	Fiber Optic Cable						X		X		X	X	X		

TABLE V. LIST OF PRE- AND POST MEASUREMENTS

	Optical Inspection	Weight	Absorptivity	Emissivity	Post Test Cross-Section	Particle Count	Attenuation Measurements
Paint	X	X	X	X			
Flex Cable	X	X			X		
M55J Composite	X	X					
HEPA Filter	X					X	
Fiber Optic Cable	X						X

TABLE VI. SAMPLES CONFIGURATIONS

	Erosion Rig	Gravelometer	Gas Gun
S13 Paint	25.4 mm x 25.4 mm	101.6 mm x 152.4 mm	76.2 mm x 127 mm
Aptek 2711 (2017)	25.4 mm x 25.4 mm	NO TEST	NO TEST
Aptek 2711 (MSL 2008)	76.2 mm x 76.2 mm	NO TEST	NO TEST
S13/Xylene Paint	101.6 mm x 101.6 mm	101.6 mm x 101.6 mm	NO TEST
Flex Cable	25.4 mm x 25.4 mm	101.6 mm x 152.4 mm	76.2 mm x 127 mm
M55J Composite	25.4 mm x 25.4 mm	101.6 mm x 152.4 mm	76.2 mm x 127 mm
HEPA Filter	177mm x 145.29mm	20.07 mm x 44.96 mm	NO TEST

Fiber Optic Cable	Special Set Up	NO TEST	Special Set Up
-------------------	----------------	---------	----------------

## VI. TEST PROCEDURE

### A. S13 Paint

Paint coupons are tested with various particle velocities, impact angles, and particle sizes. Each paint coupon is weighed before and after each test to determine the mass change during the test (a combination of paint erosion and particle embedment). Following testing, optical properties are measured and microscopic observations are made at high magnification. In order to determine the worst environment for the paint, first, the particle size and velocity

was kept constant to determine the worst case angle, 30°, 60°, or 90°.

Based on the results shown in Fig. 13, 30° was determined to be the worst impact angle, and all subsequent tests were conducted with this angle of impact. At a 30° impact angle, the sand is easily embedded into the soft silicone paint. The embedded particles darken the paint, thus increasing the absorption (Figs 14-15). Fig. 16 shows a graph of  $\alpha/\epsilon$  vs Mass Loading for 38-44 micron particles traveling at 250 m/s. As mass loading is increased, the  $\alpha/\epsilon$  values appear to converge towards a constant value of  $\alpha/\epsilon \approx 0.55$ .  $\alpha/\epsilon$  values in this range can decrease the efficiency at which the rover can reject heat to its surroundings. The  $\alpha/\epsilon$  value is mostly dependent on absorptivity because emissivity ( $\epsilon$ ) changes very little with mass loading (Fig. 17). The sand used in this erosion test is a white/brown sand; the sand on Mars is red, thus the expected absorption value of the paint on Mars after the landing event will differ from the results presented in this work. Mars simulant sand was not used for this test campaign due to facility concerns, though is an open area of investigation for future work.

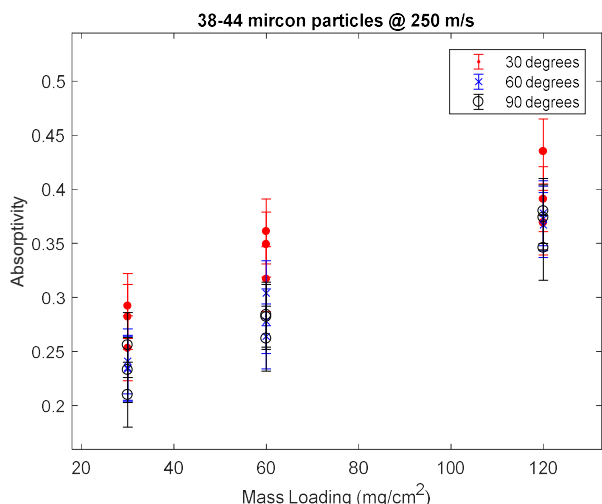


Fig. 13. Absorptivity vs. Mass Loading for 3-44 micron particles traveling at 250 m/s at different impact angles. The rate of change for absorptivity at 30° impact angle is higher than 60° and 90°. The error bars are the error margin of the instrument used, a TESA 2000 (AZ Technology).



Fig. 14. S13 coupon discolored after exposure to 38-44 micron particles traveling at 250 m/s. The left image is a virgin paint sample, the middle image is taken after 120 mg/cm² of particle exposure, and the right image is taken after 2000 mg/cm² exposure. The exposed area is ~2 cm in diameter.



Fig. 15. High magnification image of a virgin S13 sample (left). High magnification image of S13 paint with 177-250 micron particles embedded (right).

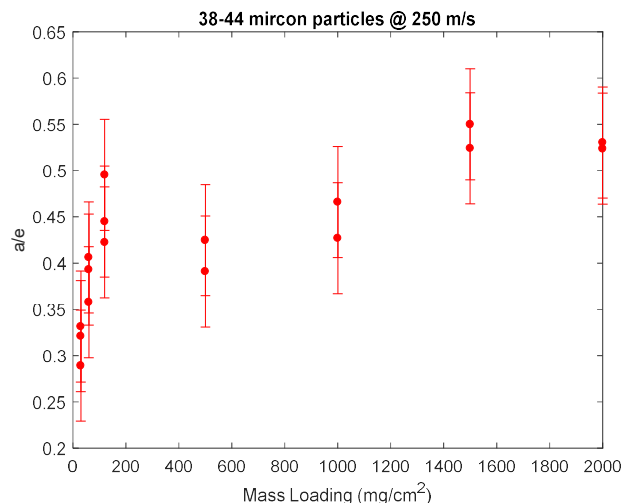


Fig. 16.  $\alpha/\epsilon$  vs Mass Loading for 38-44 micron particles traveling at 250 m/s. The  $\alpha/\epsilon$  values appear to reach a somewhat constant value at  $\alpha/\epsilon \approx 0.55$ .

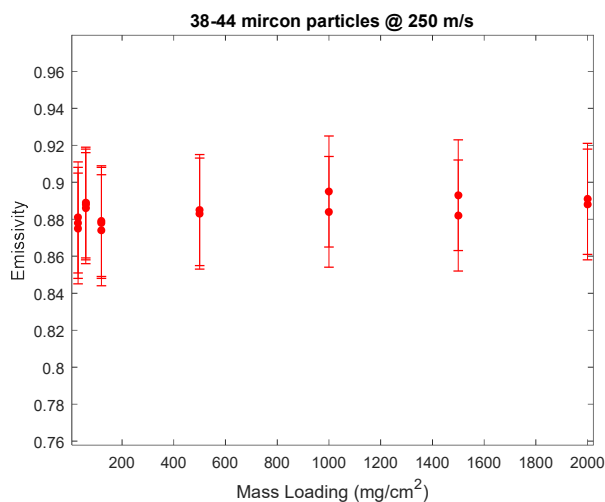


Fig. 17. Emissivity vs. Mass Loading for 38-44 micron particles at 250 m/s. Mass Loading has little effect on emissivity for all parameters.

177-250 micron sand with a velocity of 160 m/s is observed to cause linear erosion until a mass loss of ~18.5% of the initial weight (Fig. 18) is reached, at which point catastrophic adhesion failure occurs, resulting in exposure of bare aluminum (Fig. 19). The failure mode of the S13 paint is an adhesive failure to the aluminum substrate. After the paint fails, the paint chips are recovered and examined. The largest paint chip found is ~89.03 mm², which is ~24% of the exposed surface area. Before the paint failed, the  $\alpha/\epsilon$

measurements appear to reach a constant value. The new xylene thinner coupons have a higher  $\alpha/\epsilon$  value than the flight certified S13 coupons (Fig. 20). Neither the paint with 4155-xylene nor the paint with 4044-xylene experience catastrophic failure (e.g. bare aluminum) when exposed to the same particle conditions, (177-250 micron sand with a velocity of 160 m/s), but the paint did start to blister. Fig. 21 shows the effect of particle velocity on mass loss, by showing results for two tests with the same sized particles yet different velocities. Increased kinetic energy of the impacting particles (higher velocity) increases the mass loss for a given mass loading.

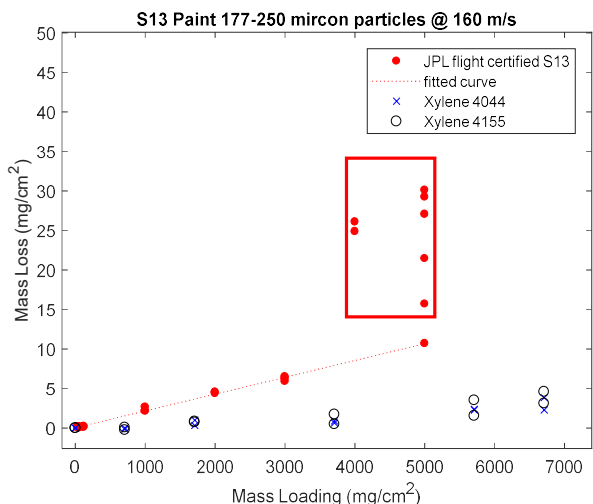


Fig. 18. The red box shows where the catastrophic failure occurred for the S13 paint. The xylene thinners did not fail.



Fig. 19. The image on the left was taken after the S13 paint coupon exposed to 177-250 micron particles at 160 m/s after 5 g/cm<sup>2</sup> mass loading. The image on the right is a paint chip found in the sand after testing.

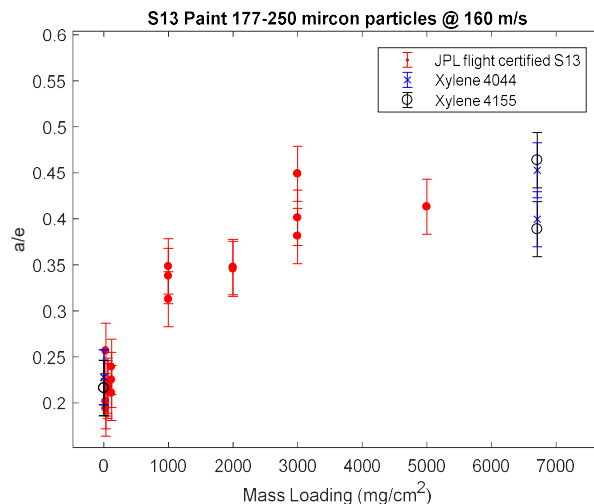


Fig. 20. The  $\alpha/\epsilon$  measurements leveled off, this data was fit with a curve. The new xylene thinner coupons had a higher  $\alpha/\epsilon$  value than the flight certified S13.

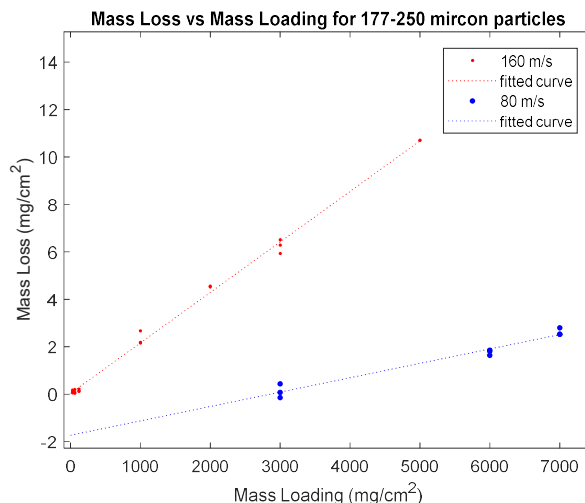


Fig. 21. This graph shows the difference in energy has on erosion. Increased velocity results in a significant increase in erosion rate for a constant particle size.

Aptek 2711 was tested along with the S13 in order to act as a control sample to compare current measurements to measurements previously taken in 2008 [3]. The Aptek 2711 samples tested in this campaign have consistent optical properties as the samples measured in 2008 (Fig. 22). However, the mass loss varied significantly between the MSL and current testing, and it is believed that this discrepancy is due to the difference in thickness of paint on the samples from 2008 compared to the current samples. When exposed to the same environment (177-250 micron sand with a velocity of 160 m/s and a 30° impact angle), the Aptek 2711 lost mass more rapidly than the S13. The Aptek 2711 failed cohesively, unlike the S13, leaving a thin layer of inorganic material behind. When exposed to enough mass loading, the Aptek 2711 was completely removed from the aluminum substrate (Fig. 23). On the MSL rover, there is only one documented location where there is evidence of paint damage (Fig. 10), and the cause of this damage is unknown.

As there are no images taken by MSL's cameras that show similar paint erosion to that shown in Fig. 23, it is believed that the test environment is more severe than the particle environment that MSL experienced while landing on Mars.

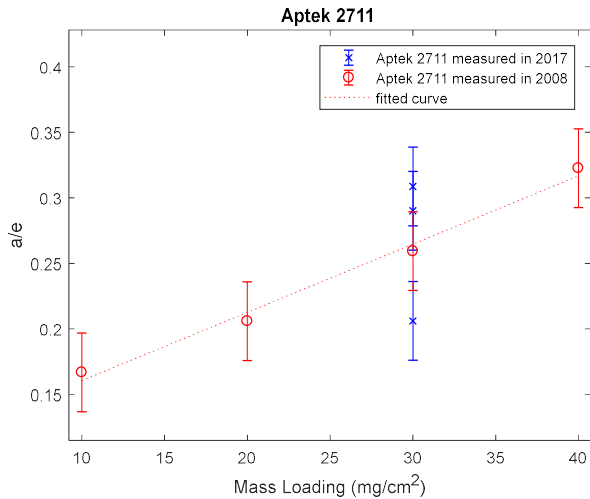


Fig. 22.  $\alpha/\epsilon$  ratio for the Aptek paint tested in 2008 for MSL compared to the Aptek paint tested in 2017 for M2020. The  $\alpha/\epsilon$  matches consistently with the margin of error from the optical instrument. Aptek 2711 was used as a control sample to confirm the M2020 paint was not over-tested and compare to the results from MSL testing [3].

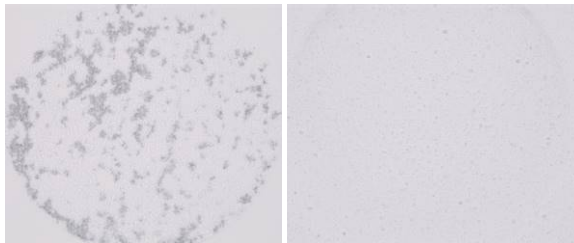


Fig. 23. Aptek 2711 coupon from MSL (left) and S-13 coupon (right) exposed to the same environment. The Aptek 2711 paint shows a cohesive failure early in testing and the S13 seems visually unaffected.



Fig. 24. Aptek paints 2706, 2719, and 2727 exposed to the same environment. 2706 had the lowest mass loss of all the Aptek samples.

The S13 paint coupons exposed to gravel gain mass linearly, as the 1-10 mm gravel breaks upon impact and embeds into the paint (Fig. 25). This contrasts an erosion mechanism. The samples gain >1% mass, followed by catastrophic failure resulting in bare aluminum (Fig. 26). Neither the paint with 4155-xylene nor the paint with 4044-xylene show bare aluminum when exposed to the same environments, but the paint did start to blister. The 25 m/s gravelometer test is performed at the lowest possible particle velocity that the test equipment allows.  $\alpha/\epsilon$  values after

gravel exposure reach a relatively constant value of  $\alpha/\epsilon \approx 0.35$ , which would only yield a modest temperature increase (Fig. 27). The impact angle of the gravelometer is fixed at 90°, but absorptivity is expected to be higher with lower impact angles (as discussed previously with respect to the Particle Erosion Rig).



Fig. 25. Optical images (low and high magnification) of the S13 after exposure to the gravelometer. The paint also appears more red compared to the Particle Erosion Rig samples due to the red color of the MMS.

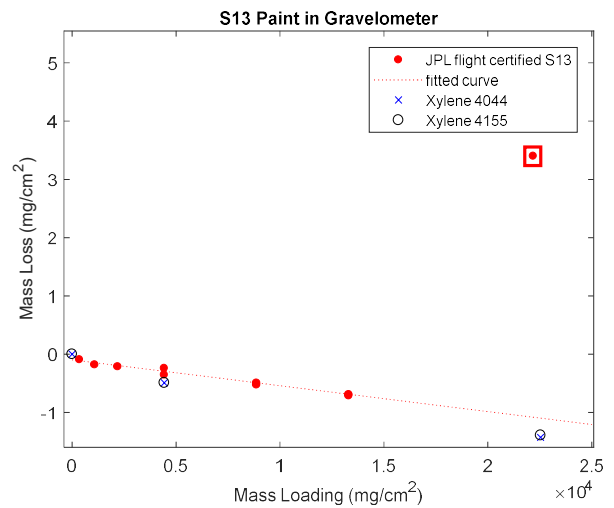


Fig. 26. In the gravelometer, the S13 gained mass linearly until catastrophic failure (red box),

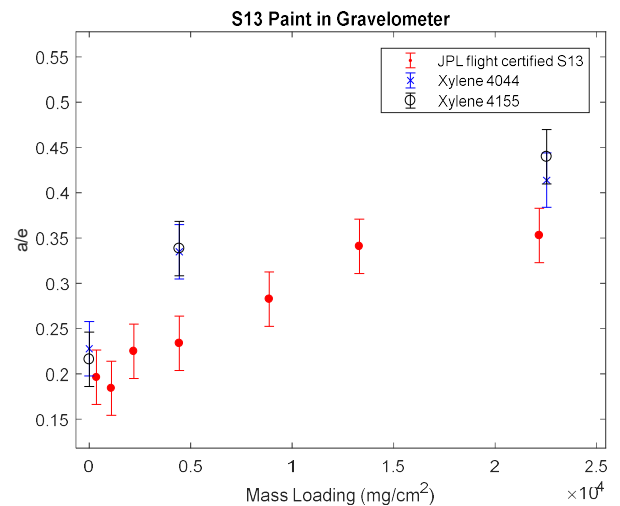


Fig. 27.  $\alpha/\epsilon$  levels off around 0.35 after exposure with the gravelometer. The samples with xylene thinners had a higher  $\alpha/\epsilon$  than the JPL certified paint.

The gas gun impact angle is variable and tests are performed at both 30° and 90°. Little damage is done to the S13 sample with a 90° impact angle. However, an impact angle of 30° causes the paint to peel away from the substrate (Fig. 28). Since the paint remains attached to the substrate in both experiments, and the color does not change significantly, there is no significant change to the emissivity and absorptivity of the paint.

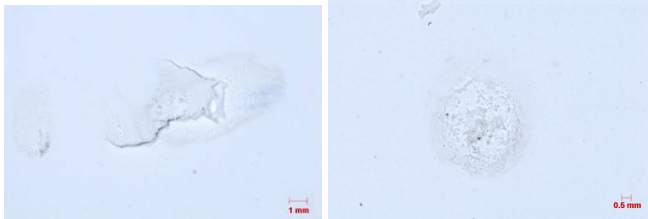


Fig. 28. Images post 15.8 mm particle impact with the Gas Gun. The impact angle of the left image is 30° and the impact angle of the right image is 90°.

### B. Flex Cable

The flex cable is tested in two different configurations: one with a piece of aluminum behind the flex cable, and a second configuration with a soft material, e.g. cardboard, mounted to it. These configurations are representative of the expected interfaces on the M2020 rover - the flex cable can be mounted directly to the rover (rigid backing), or stacked on top of multiple layers of cabling (compliant backing). After testing, the flex cable is cross-sectioned rather than functionally tested, to inspect whether the copper traces have been damaged. In particular, evidence of either shorting traces together or a fully broken open trace are indicators of a damaged flex cable. Optical imaging shows that the Kapton erodes away in some areas, but no metal traces are visible at high magnification (Fig. 29-30). The cross-section does show that the traces are deformed at the location of particle impact, but still do not make contact with the traces below, (Fig. 31). The material behind the flex cable directly affects the impact damage; aluminum backing resulted in crushed traces more often than cardboard (Figs 32-34). When the flex cable has a softer backing, the backing is able to absorb some of the impact energy. In flight, the configuration will consist of varying layers of flex cables stacked on top of each other, which will likely produce results in-between these two test configurations. Aluminum behind the flex cable is a worst-case situation and produced the most damage, but the particle impact still did not create a short or an open circuit.

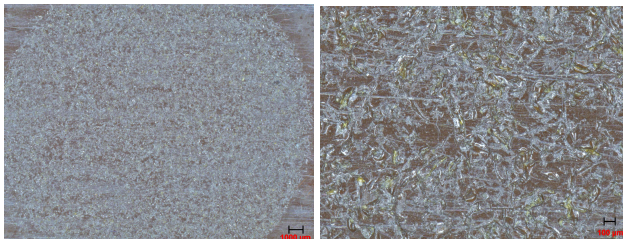


Fig. 29. When exposed to particles from 38-550 microns, in the Particle Erosion Rig, the outer layer of Kapton is abraded, but there is no damage to the traces. The left image is at low magnification and the right at high magnification.

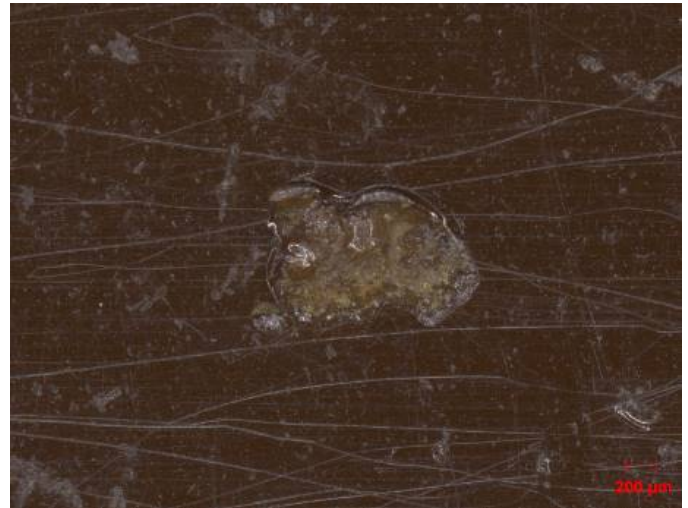


Fig. 30. Flex cable when exposed to 1-10 mm particles, in the gravelometer, the outer layer of Kapton is abraded; however, the copper traces were not exposed.

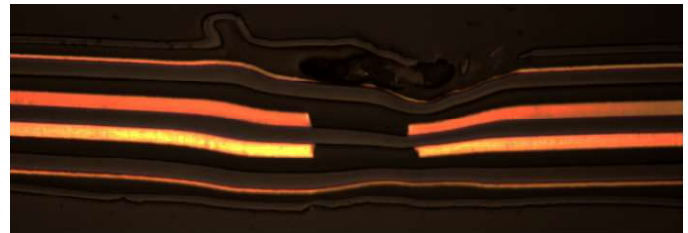


Fig. 31. Flex cable cross-section image at high magnification of the Fig. 30 location, the copper traces below the Kapton were deformed.



Fig. 32. This is an image of the flex cable after impacts from the Gas Gun. The indentation on the left is from impact with a cardboard backing and the indentation on the right is from impact with an aluminum backing.



Fig. 33. Flex cable cross-section of the indentation with a 15.8 mm particle at 24.1 m/s when there was cardboard behind the flex cable, left indentation in Fig. 32.

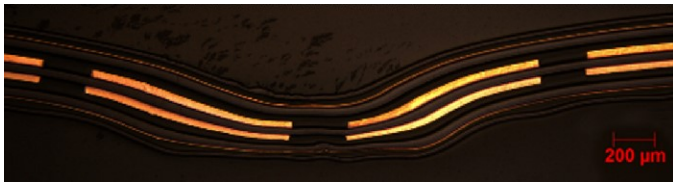


Fig. 34. Flex cable cross-section of the indentation that occurred with the same parameters but instead aluminum was behind the flex cable, right indentation in Fig. 32.

### C. Fiber Optic Cable

In order for the fiber optic cable (FOC) to be in a flight-like configuration (slack and without backing), ground support equipment (GSE) is designed to hold the FOC during testing (Fig. 35). Functional testing is performed after each particle exposure to verify that a laser can transmit light through the FOC. Videos are taken of the FOC during testing to monitor the FOC movement, and no anomalies were noted while in the Particle Erosion Rig. The FOCs that were exposed to sand passed the functional tests and no erosion was observed on the FOC. Videos taken during the Gas Gun impacts observed SN 271 deforming elastically approximately 5 cm (2 inches) after impact from a 15.8 mm particle traveling at 24.1 m/s. This level of deformation is commensurate with the acceptable bend radius of the fiber. After the deformation, the functional test had noticeably-reduced transmission through the FOC. The other FOC tested with particles smaller than 15.8 mm also deformed elastically, though less than SN 271. Post-testing attenuation measurements as a function of wavelength from 240-860 nm are also performed. In order to measure unsaturated data over the whole range of wavelengths considered, three measurements were taken: 0.8ms from 551-860 nm, 2.2ms 360-550 nm, and 5.6ms 240-395 nm. The test schematic for the attenuation measurements is shown in Fig. 36. All cables, except for SN 271 pass the requirement provided by the project. For SN 271 the attenuation was measured to be greater than the maximum allowed attenuation (Fig. 37). This FOC was tested to above the M2020 requirements.



Fig. 35. Images of the back and front of the GSE with the FOC mounted to it prior to Gas Gun testing.

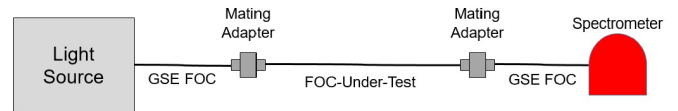


Fig. 36. To test the attenuation of the FOC one GSE FOC was connected to the light source and another GSE FOC was connected to the spectrometer these 2 GSE cables were connect to produce baseline measurements. Then the FOC that underwent erosion testing were connected in-between the GSE cables and any differences are recorded.

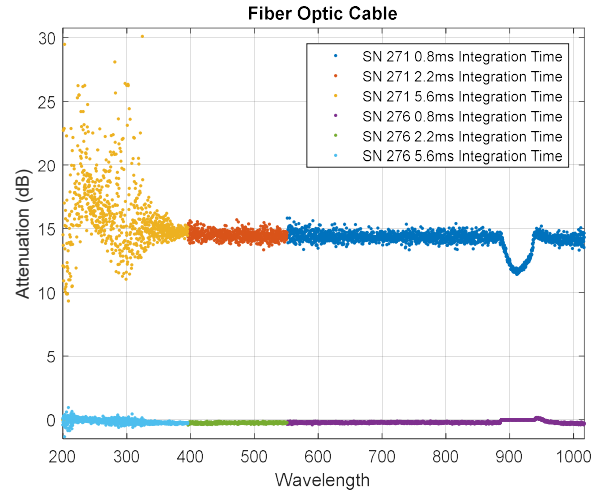


Fig. 37. The attenuation of SN 276 is an example of a FOC with acceptable attenuation and SN 271 is an example of a FOC with unacceptably high attenuation. Attenuation this high would lead to instrument failure.

### D. M55J Composite

The resin in the M55J composite started to erode after exposure to sand, but no fiber damage was visible (Fig. 38). In the gravimeter, impacts resulted in fiber damage and through-thickness holes (Fig. 39). When the composite is exposed to rock impacts, plastic deformation is observed. The maximum deformation is about 1.27 cm (0.3 inch); this occurred after two impacts of a 15.8 mm particle with a 24 m/s impact velocity (Fig. 40).



Fig. 38. Low and High magnification images of erosion of the M55J with sand. The resin has started to erode, but he fibers are still intact.



Fig. 39. Erosion of the M55J with gravel, after high mass loadings the fibers started to break and small holes were formed.



Fig. 40. Impact with two 15.8 mm particles caused the M55J to deform about 7.62 mm.

### E. HEPA Filter

Two flight HEPA filters are tested: 177.54 mm x 145.4 mm from the Rover Chassis (Fig. 41) and 30 mm x 32 mm from the RSM. Since there are a limited number of HEPA filters to test, the Rover Chassis is divided into 9 sections (Fig. 42). Each section is tested with different parameters, while the other sections are covered. The purpose of this configuration is to still be able to determine when a failure of a filter occurs, if one were to occur. After testing with the Particle Erosion Rig, the filters are inspected, and no sign of visible damage was noted. Some sand particles became trapped behind the screen, but none passed through the filter. The RSM HEPA filter is impacted with gravel traveling at 25 m/s. After an exposure of about 4700 mg/cm<sup>2</sup>, the screen over the filter showed visible

damage to the screen but none to the HEPA material as the screen blocks most of the particles (Fig. 43).



Fig. 41. The HEPA Rover Chassis mounted to a GSE plate testing with the Particle Erosion Rig.

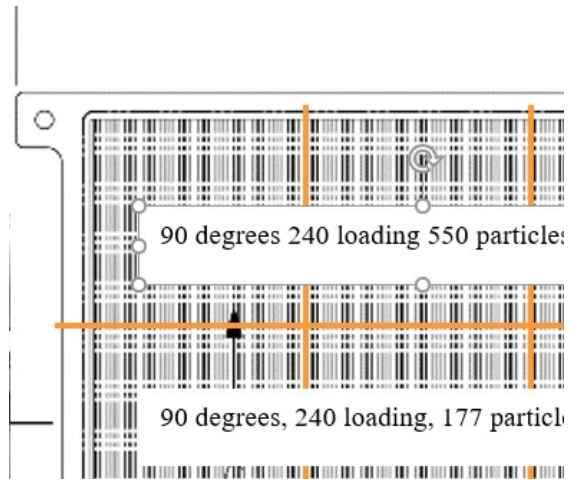


Fig. 42. Due to the limited amount of filters, the large filter was divided into 9 sections (in hopes that if the HEPA material failed the test parameter would be able to be determined based on the location of the failure.)



Fig. 43. Since the particles in the gravelometer ranged from 1-10 mm not all particles were able to pass through the 2 mm hole screen. These large particles deformed the screen on the RSM filter, but were unable to damage the filter.

In order to quantify possible damage to the HEPA filters, post- and pre-testing for this hardware includes a particle count leak check, which determines how well the HEPA filters perform. The pre- and post-test values can be compared to determine if there is any degradation in performance. In order to measure this, first, the particle counter pulls a vacuum in “dirty air” and counts how many particles of a certain size make it to the detector, which is the baseline measurement. By placing the HEPA filter in front of the detector this should decrease the baseline measurement to significantly less than the original background measurement (Fig. 44). Both filters allowed less than 0.03% of the 0.3 micron size particles through, and these results are shown in Table VII.

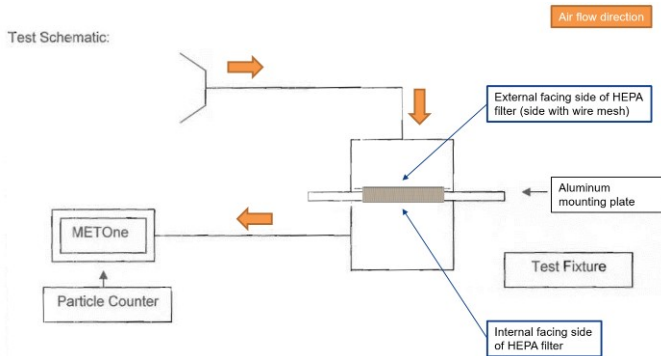


Fig. 44. HEPA filter leak check test schematic.

TABLE VII. POST TEST LEAK CHECK RESULTS

Rover Chassis HEPA Filter Post-Test Measurement		
Time	Particle Count	
Minute	0.3 $\mu\text{m}$	0.5 $\mu\text{m}$
1	2	0
2	6	0
3	1	0
4	0	0
5	8	0
Average	3.4	0
Result	PASS	
Highest Value	8	

Remote Sensing Mast(RSM) Chassis HEPA Filter Post-Test Measurement		
Time	Particle Count	
Minute	0.3 $\mu\text{m}$	0.5 $\mu\text{m}$
1	23	4
2	14	3
3	13	0
4	16	0
5	19	0
Average	17	1.4
Result	PASS	
Highest Value	23	

## VII. CONCLUSION

Based on the post-test analysis performed, it is predicted that all material tested in this work will survive the high-velocity particle environment that the M2020 rover is expected to be exposed to when it lands on Mars. Testing

was not only performed to project requirements, but also included some testing to failure in order to characterize materials for future missions that may include for severe dust environments.

An increase in the  $\alpha/\epsilon$  ratio due to particle embedment for the S13 paint was observed, and this change in optical properties needs to be accounted for in a system level thermal analysis. Once particles are embedded in the paint, there is a low likelihood of the particles migrating off of the painted surface, which means that the increased  $\alpha/\epsilon$  ratio will likely remain, and will not improve over time (unlike what has been observed on MSL). The paint with 4155-xylene and 4044-xylene were able to withstand higher velocities and mass loading than the current M2020 paint. However they have a higher  $\alpha/\epsilon$  value. Due to the high survivability of Aptek 2706 or 2719, these paints maybe considered for future missions, if the application is acceptable. This series of tests confirms that the M2020 materials are built to withstand the extreme environment that the MLEs are expected produce when landing on Mars.

## ACKNOWLEDGMENT

This testing was performed by the Jet Propulsion Laboratory, California Institute of Technology, under contract with NASA at UDRI. Thank you to Cheryl Castro, Kevin Poormon, and Matt Rothgeb for test facility operation and data acquisition support.

## REFERENCES

- [1] Vizcaino, Jeffrey, and Manish Mehta. “Quantification of Plume-Soil Interaction and Excavation Due to the Mars Science Laboratory Sky Crane Descent Phase.” *8th Symposium on Space Resource Utilization*, Feb. 2015, doi:10.2514/6.2015-1649.
- [2] M. Schoenenberger, A. Dyakonov, P. Buning, W. Scallion, and J. Van Norman. Aerodynamic challenges for the Mars Science Laboratory entry descent and landing, in: 41st AIAA Thermophysics Conference, 22–25 June, San Antonio, Texas, 2009.
- [3] Sengupta, Anita, J. Kulleck, J. Van Norman, and M. Mehta. “Thermal Coating Erosion in a Simulated Martian Landing Environment.” *Wear*, vol. 270, no. 5-6, 2011, pp. 335–343., doi:10.1016/j.wear.2010.09.013.
- [4] “Raw Images - Mars Science Laboratory.” *NASA*, NASA, mars.nasa.gov/msl/multimedia/raw/.
- [5] Hutton, Rober. *Mar Surface EROsion Study*. 1968.
- [6] Hutton, R. E., H. J. Moore, R.F. Scott, R. W. Shorthill, and C. R. Spitzer. “Surface Erosion Caused on Mars from Viking Descent Engine Plume.” *The Moon and the Planets*, vol. 23, no. 3, 1980, pp. 293–305.
- [7] Roberts, L.: 1968, 'The interaction of a rocket exhaust with the lunar surface', in *The Fluid Dynamics Aspects of Space Flight*, Gordon and Breach Inc., New York, v. 2.
- [8] Chen, Curtis W., and Brian D. Pollard. “Radar Terminal Descent Sensor Performance During Mars Science Laboratory Landing.” *Journal of Spacecraft and Rockets*, vol. 51, no. 4, 2014, pp. 1208–1216.
- [9] “MIL-STD-3033 Particle/Sand Erosion Testing of Rotor Blade Protective Materials.” *Department of Defense Test Method Standard*, 28 July 2010.
- [10] *Particle Erosion Test Apparatus*. University of Dayton Research Institute, 2012. udayton.edu/udri/capabilities/materials/particle\_erosion

- [11] “D3170 Test Method for Chipping Resistance of Coatings.” *ASTM International*.
- [12] Grossman, D M, S. J. Grossman, G. J. Billington. “Patent US6679095 - Multi-Test Gravelometer.” *Google Patents*, Google, Jan. 2004, [google.com/patents/US6679095](https://google.com/patents/US6679095).
- [13] Peters, Gregory H., G. Bearman, G. Mungas. “Mojave Mars Simulant--Characterization of a New Geologic Mars Analog.” *Icarus*, vol. 197, no. 2, 2008, pp. 470–479., doi:10.1016/j.icarus.2008.05.004
- [14] “Rover - Mars 2020 Rover.” *NASA*, NASA, [mars.nasa.gov/mars2020/mission/rover/](https://mars.nasa.gov/mars2020/mission/rover/)